Crystalline Polymorphism and Phase Transition Behavior of Mesogenic 4-Heptyloxy-4′-cyanobiphenyl (7OCB)

Kayako Hori,* Yoshiko Koma, Minako Kurosaki, Koichi Itoh,† Hidehiro Uekusa,††

Yasuyuki Takenaka,†† and Yuji Ohashi††

Department of Chemistry, Ochanomizu University, Otsuka, Bunkyo-ku, Tokyo 112

†Department of Chemistry, School of Science and Engineering, Waseda University, Okubo, Shinjuku-ku, Tokyo 169

††Department of Chemistry, Tokyo Institute of Technology, O-okayama, Meguro-ku, Tokyo 152

(Received August 31, 1995)

Four different solid phases were found for the title compound: square-plate and needle crystals, which are metastable, a solid found in a collapsed plate crystal and the most stable crystalline phase found in a commercially available powder specimen. The phase transition behavior of each solid to the nematic phase was investigated by DSC. The phase relations are proposed in terms of Gibbs energy and temperature diagram. The structure of the plate crystal has been determined at 243 K. The crystal has a distinct smectic-like structure composed of bilayers. The CN groups are closely arranged between antiparallel molecules within a bilayer, resulting in infinite networks with the C–N distances; 3.41—3.64 Å.

Series of 4-alkyl-4′-cyanobiphenyl (*n*CB) and 4-alkoxy-4′-cyanobiphenyl (*n*OCB) have been widely studied[1] as useful mesogens with simple molecular structures. Both series have similar phase sequences: crystal-nematic-isotropic for $n=$ 1—7 (monotropic nematic for $n=1$—4), crystal-smectic A-nematic-isotropic for $n=8, 9$ (and 11CB), and crystal-smectic A-isotropic for $n\geq 10$ (except for 11CB).[2] Smectic phases are dominant over the nematic phase for longer chain members in many homologous series.

Since a very early work of Bernal and Crowfoot,[3] a number of crystal structures of mesogens have been determined and discussed in relation to the liquid crystalline behavior. As for the crystal structures of the series, those of lower homologues ($n=1$—5) for *n*CB[4—7] and *n*OCB[8,9] have been reported. In the course of systematic single crystal X-ray analysis for longer chain members of *n*OCB, we found four different solid phases for 7OCB. The polymorphism results from the subtle balance of various kinds of intermolecular interactions. So, it may give us some information about the intermolecular interactions controlling the mesophase behavior to know the precise molecular arrangements of the polymorphs and their thermodynamic relations. One of the crystal structures, the needle crystal, has already been reported together with that of 6OCB.[10] This paper describes the crystal structure of another phase (the square-plate crystal) and the phase transition behavior of the polymorphs studied by differential scanning calorimetry (DSC).

Experimental

Material. 7OCB was purchased from BDH Chemicals Ltd. Slow evaporation of solvents from an acetone–water or a diethyl ether–methanol solution at about 5 °C gave transparent square-plate crystals in most cases. However, needle crystals were also grown in a similar condition. Mostly, the two forms were obtained separately. The ratio of ocurrence of the latter was about 10% or less. The square-plate crystals were sometimes very thin with iridescent color but typically of the order of 0.1 mm. The dimensions of edges were sometimes as long as several mm. The needle crystals were typically of the order of 0.1 mm in width and several mm in length.

Apparata. DSC mesurements were carried out on Seiko SSC570 and DSC22C calorimeters. Special attention was paid to select transparent crystals under a microscope, since the crystals were metastable phases, as described below. The relative errors for ΔH values were estimated to be 2—10%. Microscopic observation of the square-plate crystals on heating process was done on an Olympus POM microscope equipped with a Mettler FP82 hostage. Powder X-ray diffraction patterns were obtained on a Rigaku RAD-RA diffractometer.

Single Crystal X-Ray Analysis. Since the plate crystal collapses too rapidly to obtain X-ray data at room temperature, all the X-ray experiments on a single crystal were carried out at −30 °C. Accurate cell parameters were determined by a least-squares fit for 25 reflections within the range, $58<2\theta<60°$, measured on a Rigaku AFC-5R diffractometer with Cu $K\alpha$ radiation ($\lambda=1.54184$ Å) monochromated by graphite. Intensity data were measured on the diffractometer using a crystal of $0.4\times0.3\times0.02$ mm up to $2\theta=125°$. An ω scan mode with a scan rate of 16° min^{-1} was applied. Three standard reflections were recorded after every 100 reflections. No significant intensity variations were observed. The data were corrected for Lorentz and polarization factors but not for absorption.

Totally 5823 unique reflections were collected. Systematic absences, $l=2n+1$ in $h0l$ and $k=2n+1$ in $0k0$, were observed. Furthermore, reflections $h+k=2n+1$ in hkl were relatively weak; $\langle I/\sigma(I)\rangle=1.5$ for $h+k=2n+1$ and 17.5 for $h+k=2n$. Only 14% of the reflections for $h+k=2n+1$ had $I>2\sigma(I)$, in which 1% had $I>20\sigma(I)$, while 76% of the reflections for $h+k=2n$ had

$I > 2\sigma(I)$, in which about 10% had $I > 50\sigma(I)$, suggesting that the structure has an approximate symmetry of *C*2/*c*. We first solved the structure by assuming the space group of $P2_1/c$ and the refinement by using SHELX76[11] converged to $R = 0.094$. In the resultant structure, however, two crystallographically independent molecules were highly symmetric with a pseudo-inversion between them. Thus, we redetermined the structure with the space group of *C*2/*c*, by using SAPI90[12] for solving and SHELXL93[13] for refinement. This is regarded as a case of the 'notorious' problem of pseudo-symmetry.[14] Crystal data; 4-heptyloxy-4′-cyanobiphenyl, $C_{20}H_{23}ON$, $M_r = 293.39$, monoclinic *C*2/*c* (more precisely, $P2_1/c$), $T = 243$ K, $a = 69.458(11)$, $b = 7.0442(8)$, $c = 6.8686(5)$ Å. $\beta = 92.359(9)°$, $V = 3357.8(7)$ Å^3, $Z = 8$, $d_x = 1.161$ g cm^{-3}, $F(000) = 1264$, $\mu = 5.46$ cm^{-1}.

The structure was refined on F^2 by the full-matrix least-squares method. The weighing scheme was $w = [(0.2507P)^2 + \sigma(F_o^2)^2]^{-1}$, where $P = (F_o^2 + 2F_c^2)/3$. All the nonhydrogen atoms were refined anisotropically. Hydrogen atoms, whose positional parameters were constrained to have the C–H distances of 0.99, 0.98, and 0.94 Å for primary, secodary, and aromatic C atoms, respectively, were included in the refinement. Isotropic temperature factors for the hydrogen atoms were fixed to be 1.2 times of those of the bonded C atoms. Atomic scattering factors were taken from the International Tables for Crystallography.[15] Max. Δ/σ and max. and min. $\Delta\rho$ in the final difference map were 0.00 and 0.22, −0.30 e Å^{-3}, respectively. Final $R(F)$ and $wR(F^2)$ for 2015 reflections with $|F_o| > 4\sigma(|F_o|)$ for *C*2/*c* were 0.057 and 0.180, respectively. Goodness of fit for F^2 was 0.63. Final atomic coordinates are shown in Table 1.[16]

Table 1. Final Atomic Coordinates ($\times 10^4$) with Their Estimated Standard Deviations in Parentheses and Equivalent Thermal Parameters (U_{eq}, $\times 10^3$) for the Plate Crystal of 7OCB

Atom	*x*	*y*	*z*	U_{eq}[a]/Å^2
O	6445(1)	7246(3)	10891(3)	48(1)
N	4932(1)	7416(3)	15190(3)	54(1)
C(1)	5093(1)	7432(4)	14864(3)	43(1)
C(2)	5294(1)	7468(4)	14415(3)	39(1)
C(3)	5364(1)	8994(4)	13368(3)	41(1)
C(4)	5553(1)	9024(4)	12872(3)	39(1)
C(5)	5680(1)	7542(3)	13398(3)	36(1)
C(6)	5608(1)	6049(4)	14481(3)	43(1)
C(7)	5417(1)	5996(4)	14974(3)	45(1)
C(8)	5881(1)	7547(3)	12781(3)	36(1)
C(9)	5930(1)	8397(3)	11033(4)	41(1)
C(10)	6115(1)	8366(4)	10364(4)	43(1)
C(11)	6260(1)	7443(3)	11455(4)	39(1)
C(12)	6217(1)	6634(3)	13227(3)	41(1)
C(13)	6032(1)	6675(3)	13879(3)	40(1)
C(14)	6490(1)	7904(4)	8978(4)	46(1)
C(15)	6688(1)	7180(4)	8547(4)	48(1)
C(16)	6757(1)	7870(4)	6606(4)	47(1)
C(17)	6956(1)	7148(4)	6172(4)	48(1)
C(18)	7032(1)	7848(4)	4263(4)	49(1)
C(19)	7232(1)	7146(5)	3863(4)	57(1)
C(20)	7313(1)	7917(6)	2018(5)	78(1)

a) U_{eq} is defined as one third of the traces of the orthogonalized U_{ij} tensor.

Results and Discussion

Thermal Behavior of the Polymorphs. At room temperature, the plate crystals collapsed to be opaque-white in a day or so, while the needle crystals changed much more slowly, keeping their transparency for a few months. The latter, however, became powdered on the surface after several months at room temperature. In order to study kinetic aspects of these metastable phases, DSC measurements were carried out at different heating rates. The commercial sample shows a single melting peak at the highest temperature (54 °C), which is independent of the heating rate, indicating that this solid is the most stable phase. On the other hand, other solids show more complicated curves, which depend on the heating rates.

Figure 1 shows DSC traces of the plate crystal. There are four endothermic peaks: I, II, III, and IV. As the heating rate decreases, the peaks I and II become small and the peak I shifts to the lower temperature with the flattered shape. Both peaks are undetectable at the very slow scan rate of 0.12 K min^{-1}. The DSC trace of the opaque-white solid derived from the plate crystal has only two successive endothermic peaks above 52 °C, as shown in Fig. 2. The peak profiles are similar to those of peaks III and IV of the original plate crystal. Figure 3 shows the ΔH values estimated for the plate crystal and the collapsed solid. For the former, the ΔH values of the peaks I, II, and III decrease to zero, while that of the peak IV increases, as the heating rate decreases. The two peaks of the collapsed solid show similar behavior to the peaks III and IV of the plate crystal. These facts show that the plate crystal and the collapsed solid take on a common state at the temperature just below the successive two peaks above 52 °C. It is also shown that the collapsed solid is not the completely stabilized state. Thus, we refer the state as the state-A, hereafter. The ratio of ΔH for the two peaks above 52 °C vary complimentarily with the change of the

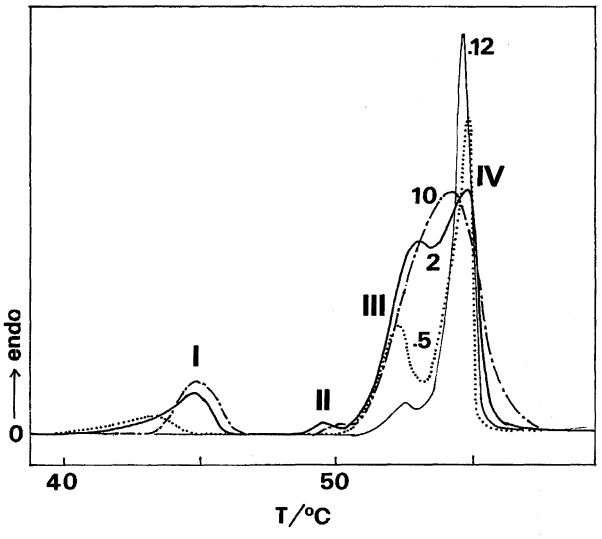

Fig. 1. DSC traces of the plate crystal at heating rates of 0.12, 0.5, 2, and 10 K min^{-1}. The numerical figures denote the heating rates. I, II, III, and IV distinguish the peaks.

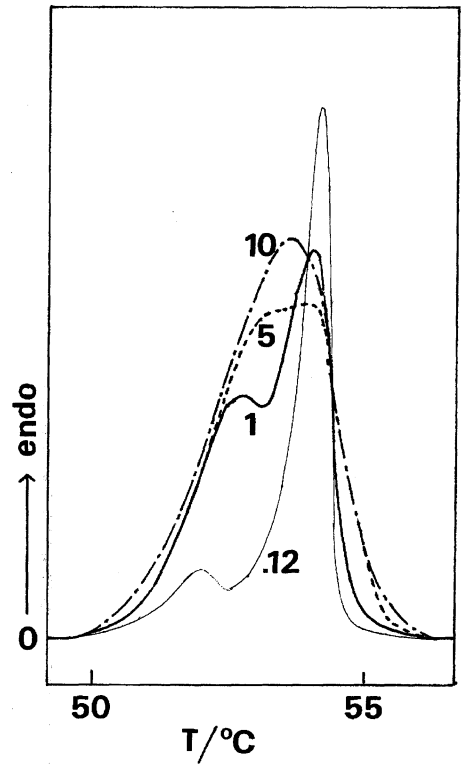

Fig. 2. DSC traces of the collapsed solid at heating rates of 0.12, 1, 5, and 10 K min^{-1}. The numerical figures denote the heating rates.

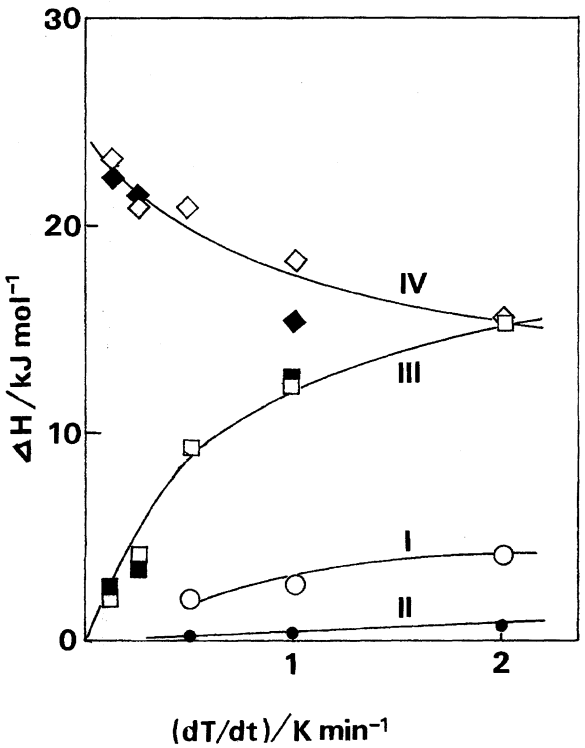

Fig. 3. Heating rate dependence of transition enthalpy change (ΔH) for the plate crystal and the collapsed solid. ○, ●, □, ◇, ■, and ◆ denote the peaks I, II, III, and IV of the plate crystal and the corresponding peaks of the collapsed solid, respectively.

heating rate. Therefore, the two peaks are associated not to a series of successive transitions but to competitive two transition processes. The higher temperature peak is situated at an almost identical point with the crystal-nematic transition peak of the commercial sample. These results indicate that the state-A consists of two phases, whose ratio is dependent on the heating rate. One corresponds to the most stable phase (called state-A′), which transforms to the nematic phase at 54 °C, while the other (called state-A″) transforms to the nematic phase at a lower temperature (near 52 °C).

Figure 4 shows DSC traces of the needle crystal. Each trace except for that at a scan rate of 5 K min^{-1} shows an endothermic peak (I) followed by an exothermic one (II) and two successive endothermic peaks (III and IV). The ΔH values for the needle crystal in Fig. 5 show a complementary relationship between the ΔH values of the peaks I and IV; i.e., the ΔH values of the peak I decreases while that of the peak IV increases monotonously, as the heating rate decreases. On the other hand, the ΔH values for the peaks II and III have maxima. The exothermic peak (II) is due to a stabilization process, which is triggered by the onset of the first endothermic transition, to a more stable state. At a scan rate of 5 K min^{-1}, there are only two endothermic peaks I and III, in which the former is overwhelmingly dominant, showing

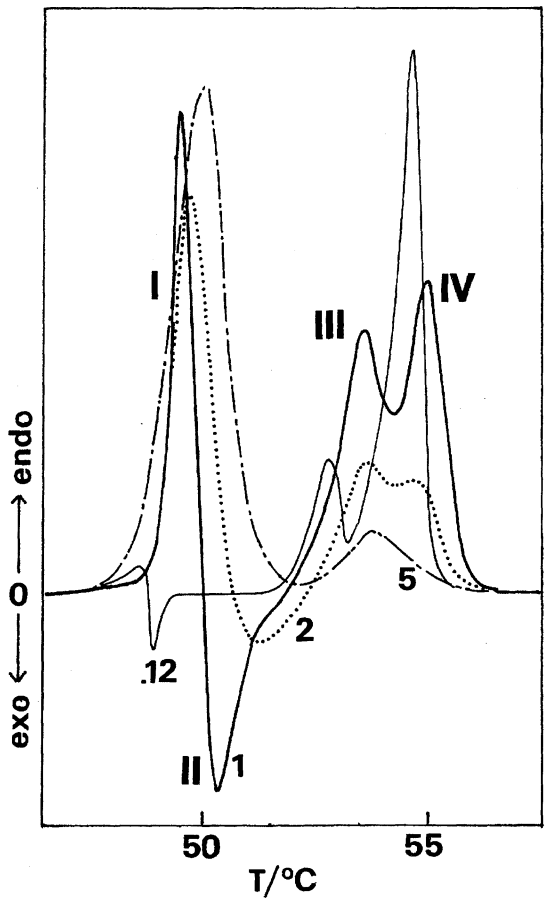

Fig. 4. DSC traces of the needle crystal at heating rates of 0.12, 1, 2, and 5 K min^{-1}. The numerical figures denote the heating rates. I, II, III, and IV distinguish the peaks.

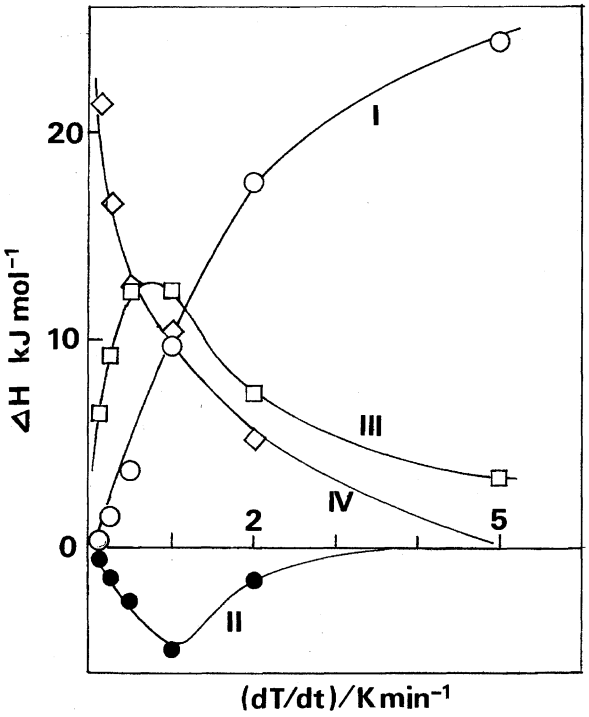

Fig. 5. Heating rate dependence of transition enthalpy charge (ΔH) for the needle crystal. ○, ●, □, and ◇ denote the peak I, II, III, and IV of the needle crystal, respectively.

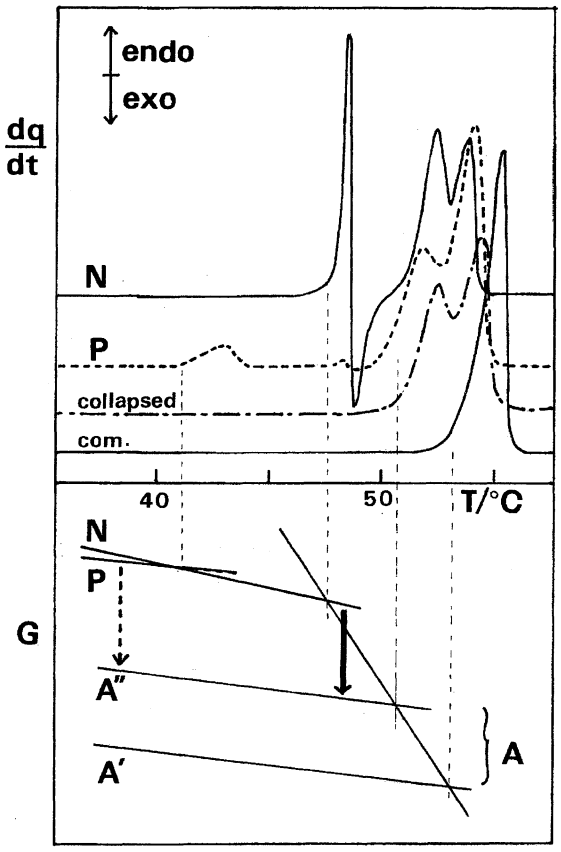

Fig. 6. DSC results at a scan rate of 1 K min^{-1} (upper) and the Gibbs energy–temperature diagram (lower). N and P in each diagram stand for the needle nad plate crystals. Collapsed solid and the commercial sample are denoted as collapsed and com., respectively, in the upper diagram. For the notations, A, A′, and A″, see text. ⟶ and - - → denote rapid and slow stabilization processes, respectively. The process from A″ to A′ is not shown, because it is not clear whether each crystal stabilizes to the states A″ and A′ at the same time or it stabilizes to the state A″ and then to the state A′.

that the peak I at about 47 °C corresponds to the crystal to nematic transition.[17] As the heating rate decreases, the stabilization process, triggered by the crystal-nematic transition, becomes significant, giving the peaks II, III, and IV. Thus, the needle crystal undergoes two competitive processes; i.e., direct transition to the nematic and the stabilization process triggered by the transition. The ratio of the two processes is dependent on the heating rate. The ΔH value of the peak IV is extrapolated to that (29 kJ mol^{-1})[2] of the most stable commercial sample, showing that the stabilization proceeds completely on extremely slow heating. Similarity in the DSC traces observed above 52 °C at slower heating rate between Figs. 2 and 4 suggests that the stabilization leads to the state-A, as in the opaque-white solid.

Phase Relations. Figure 6 shows proposed phase relations in terms of schematic diagrams of Gibbs energy vs. temperature based on the DSC data recorded at a scan rate of 1 K min^{-1}. As already mentioned, the commercial sample is the most stable. The plate crystal spontaneously collapse to the opaque-white solid, indicating that the former has higher Gibbs energy than the latter. The needle crystal transforms to the nematic at lower temperature (47.5 °C) than the states A″ and A′ do (at 52 and 54 °C, respectively) and has an exothermic stabilization process to the state A′ and A″ triggered by the onset of the transition at 47.5 °C. Therefore, the needle crystal also has higher Gibbs energy than the opaque-white solid. The stabilization process is shown by a bold arrow in Fig. 6.

On the other hand, the plate crystal stabilizes little by little even at room temperature, which is shown by a broken arrow. Presumably, the process is so slow that the evolution of heat can not be detected by DSC. Both the needle and the plate crystals stabilize not only to the most stable phase (A′) but also to the metastable phase (A″), whose ratio is dependent on the heating rate, as indicated by the complementary relation of ΔH associated to the higher-temperature two peaks. However, it is not clear whether they stabilize to the two states at the same time or they transform first to the state A″ and then to the state A′. The plate crystal shows another broad endothermic peak in the region of 33—43 °C, which corresponds to the peak I in Fig. 1. The broadness of the peak and the beginning temperature of the peak are strongly dependent on the scanning rate, as shown in Fig. 1. This fact suggests the possibility that the equilibrium transition temperature is still lower than that shown in this figure. Microscopic observation shows that spherulitic crystallites begin to grow at about 30 °C in a single plate crystal. Therefore, this broad peak corresponds to the transition from the

plate crystal to a higher-temperature crystalline phase. The peak II is attributable to the transition point of the higher-temperature solid to the nematic phase, because the ΔH value of this peak, though very small, increases slightly as the heating rate increases, as shown in Fig. 3. This is interpreted as showing that most of the labile plate crystal has stabilized to the state A and only a small portion of the higher-temperature phase of the plate crystal survives when the sample is heated to the peak II, especially at a slower heating rate. It is also pointed out that the peak II of the plate crystal is found at almost the same temperature (47.5 °C) as the peak I of the needle crystal, suggesting that the higher-temperature phase of the plate crystal is the needle crystal.

These DSC results show that there are at least four solid phases for 7OCB, the plate and the needle crystals, the most stable phase in the commercial sample (A′), and an intermediate state found in the collapsed plate crystal (A″). The phase relations discussed here suggest that the commercial sample is a specimen which has been completely stabilized after being kept at room temperature for long time, irrespective of the originally obtained form.

Jain et al. reported three crystalline polymorphs for 7OCB;[18] a virgin sample and those obtained by solidifying a melt at slow and rapid cooling rates. A phase obtained by slow cooling (SCII) exhibited a DSC trace similar to that of the needle crystal. Thus, it is suggested that the phase SCII corresponds to the needle crystal. They reported that a phase obtained by rapid cooling (SCI) undergoes an exothermic process in the temperature range of 33—38 °C, where SCI stabilizes to SCII, suggesting the existence of a less stable phase than the needle crystal.

Crystal Structures of the Polymorphs. As was described in the Experimental section, the plate crystal shows pseudo-symmetry. In IR spectra,[19] the plate crystal shows a symmetrical singlet band for CN stretching vibration at 2237 cm^{-1}. This strongly suggests that all the molecules are equivalent at least around the CN moiety. Nevertheless, the number of the reflections which violate the systematic absence is not negligible. Probably, the fundamental symmetry of *C2/c* would be partially broken by, for example, a stacking fault of the distinct smectic-like layer structure, described below, which could result from alteration of molecular conformation, such as the degree of the twisting of the biphenyl moiety. The partial symmetry breakdown was reproducible for another specimen of the plate crystal of 7OCB and also found for the plate crystals of 9OCB and 10OCB.[20] Thus, the pseudo-symmetry is regarded to be characteristic to the plate crystals of the series.

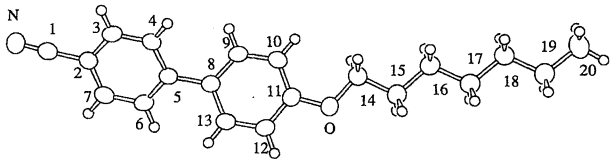

Fig. 7. ORTEP drawing with 50% thermal ellipsoids for the molecule of 7OCB with a numbering scheme.

Figure 7 shows an ORTEP drawing[21] of the molecule in the plate crystal with a numbering scheme. For the related compounds, $HO(CH_2)_nOC_6H_4C_6H_4CN$[22] ($n = 3$—11) and other biphenyls, it was found that the bond angles involving the C atoms in the biphenyl linkage deviate from the expected value, 120°. In the present crystal of 7OCB, the bond angles are slightly smaller than the ideal value, 117.6(2) and 116.5(2)° for C(4)–C(5)–C(6) and C(9)–C(8)–C(13), respectively. All other bond lengths and angles are normal within experimental errors. The molecule has a twisted biphenyl moiety with the dihedral angle of 31.1(1)° and an extended

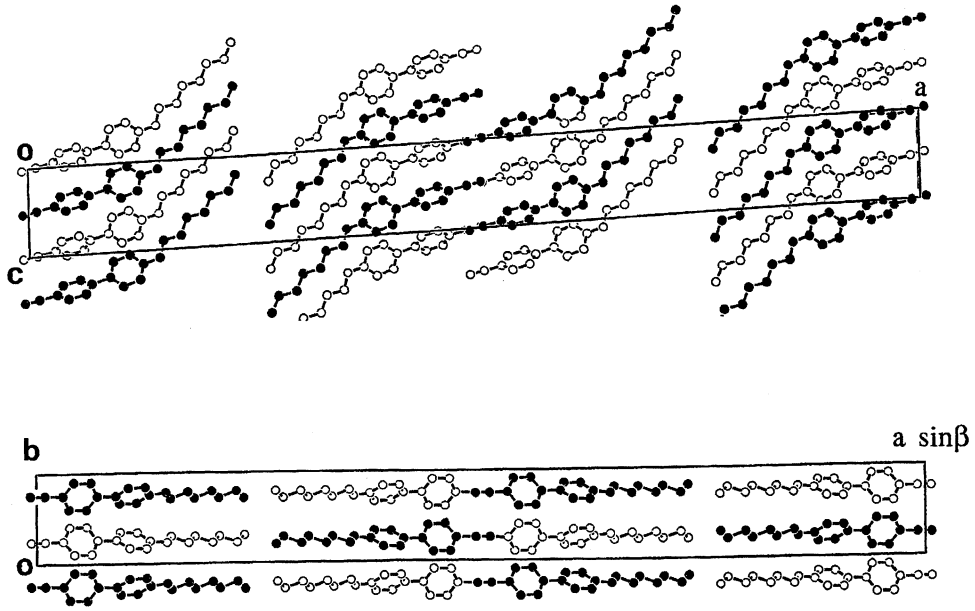

Fig. 8. Crystal structure of 7OCB viewed along the *b* axis (upper) and the *c* axis (lower). Black and white circles denote molecules of the front and back, respectively.

paraffin chain with the torsion angles within the range of 179—183°.

Figure 8 shows the structure of the plate crystal viewed along the *b* and *c* axes. The crystal has a distinct smectic-like structure composed of bilayers. The unit cell contains two bilayers. The layer plane is parallel to the *bc* plane. The tilt angle of the core moiety to the layer normal is estimated to be 20°. Paraffin chains of adjacent molecules have relatively regular arrangement with interchain distances comparable with those found in long chain compounds (4.13—4.14 and 4.20 Å[23,24]). The CN groups are closely arranged between antiparallel molecules, resulting in infinite networks with the C···N distances, 3.41—3.64 Å, as shown in Fig. 9. A similar contacts mode of CN groups was reported for $n=7$—11 of $HO(CH_2)_nOC_6H_4C_6H_4CN$.[22] In these crystals, however, each unit cell contains single bilayer.

As already reported,[10] the needle crystal has a triclinic unit cell, $T=298$ K, $P\bar{1}$, $a=12.6556(8)$, $b=19.044(2)$, $c=7.3495(5)$ Å, $\alpha=94.142(8)$, $\beta=100.108(5)$, $\gamma=91.036(7)°$, $V=1738.4(2)$ Å^3, $Z=4$. The crystal also has a smectic-like layer structure composed of crystallographically independent molecules, A and B, as shown in Fig. 10. The conformations are almost the same as that of the plate crystal with twisted biphenyl moieties (37° for A and 40° for B) and all-trans zigzag chains. Packing modes, however, are quite different from those of the plate crystal. First, close contacts of the CN groups form a dimeric arrangement (C···N distances, 3.55 and 3.39 Å), which is further paired to be a tetramer with the C···N distance of 3.57 Å, in contrast to the case of the infinite networks of the groups in the plate crystal. Secondly, the tilt angle (64°) in the smectic-like layer is larger than that of the plate crystal (20°), suggesting less lateral overlapping of molecules in the needle crystal. These facts show that intra-layer interaction is stronger in the plate crystal than that in the needle crystal.

It is of interest to know the crystal structure of the most stable phase in the commercial sample. All the attempts to obtain single crystals of this phase from a solution, however, have resulted in the formation of the metastable crystals. The

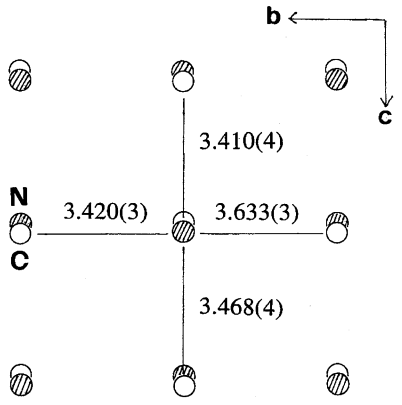

Fig. 9. Interatomic distances (Å) among CN groups. Each pair is exactly parallel, because it is related by an inversion center along the *b* axis and by a two-fold axis along the *c* axis.

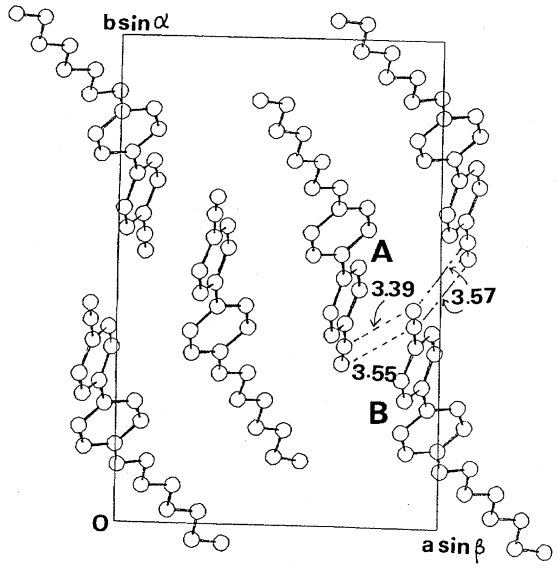

Fig. 10. The crystal structure of the needle crystal of 7OCB viewed along the *c* axis. A plane of a smectic-like layer structure, where intermolecular interaction between the terminal chains is regarded to be relatively weak, is parallel to the *ac* plane.

powder X-ray diffraction pattern of the commercial sample is shown in Fig. 11(a), which is compared with that of the plate crystal in Fig. 11(b). Intensities of diffraction peaks at lower angles are weaker than those in the higher angles in Fig. 11(a), in contrast to the case of Fig. 11(b), where the peak intensities at lower angles are greater than those at higher angles. This fact shows that a smectic-like layer structure is not prominent, suggesting a more intricate packing of molecules in the most stable phase.

Conclusions. 7OCB has at least four different solid phases: plate and needle crystals, which are metastable, the

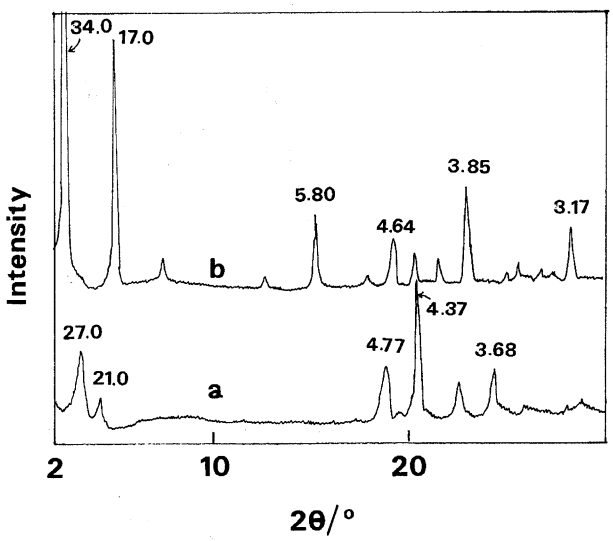

Fig. 11. X-Ray powder diffraction patterns for the commercial sample (a) and freshly powdered plate crystal (b). Numerical values at peaks are *d* values (Å).

most stable phase shown by a commercially available sample, an intermediate state found in a collapsed solid derived from the plate crystal. Crystal structures of the two forms have been compared. The plate crystal has a distinct smectic-like layer structure with infinite networks of close arrangements of CN groups, while the needle crystal has a largely tilted smectic-like layer structure with a tetrameric arrangement of CN groups. Thermodynamical phase relations are discussed on the basis of the DSC results.

This work was supported by a Grant-in-Aid from Hayashi Memorial Foundation for Female Natural Scientists to K. H.

References

1) For example: I. Ono and S. Kondo, *Bull. Chem. Soc. Jpn.*, **66**, 633 (1993).
2) BDH catalogue data.
3) J. D. Bernal and D. Crowfoot, *Trans. Faraday Soc.*, **29**, 1032 (1933).
4) W. Haase, J. Loub, and H. Paulus, *Z. Kristallogr.*, **202**, 7 (1992).
5) W. Haase, H. Paulus, and R. Pendzialek, *Mol. Cryst. Liq. Cryst.*, **100**, 211 (1983).
6) G. V. Vani, *Mol. Cryst. Liq. Cryst.*, **99**, 21 (1983).
7) T. Hanemann, W. Haase, I. Svoboda, and H. Fuess, *Liq. Cryst.*, **19**, 699 (1995).
8) L. Walz, H. Paulus, and W. Haase, *Z. Kristallogr.*, **180**, 97 (1987).
9) P. Mandal and S. Paul, *Mol. Cryst. Liq. Cryst.*, **131**, 223 (1985).
10) K. Hori, Y. Koma, A. Uchida, and Y. Ohashi, *Mol. Cryst. Liq. Cryst.*, **225**, 15 (1993).
11) G. M. Sheldrick, "SHELX76, A Program for Crystal Structure Determination," Univ. of Cambridge (1976).
12) F. Hai-Fu, "SAPI190, Structure Analysis Program," (1990).
13) G. M. Sheldrick, "SHELXL-93, A Program for the Rifinement of the Crystal Structure," Univ of Göttingen (1993).
14) R. E. Marsh and F. H. Herbstein, *Acta Crystallogr., Sect. B*, **B44**, 77 (1988), and references cited therein.
15) "International Tables for Crystallography," ed by A. J. C. Wilson, Kluwer Academic Publishers, Dordrecht (1992), Vol. C.
16) The tables of the anisotropic temperature factors for non-hydrogen atoms, bond distances and angles, the parameters of hydrogen atoms and the $F_o - F_c$ are deposited as Document No. 69015 at the Office of the Editor of Bull. Chem. Soc. Jpn.
17) This corresponds to one of two melting points, 47.5 and 54.0 °C reported by BDH in Ref. 2.
18) S. C. Jain, S. A. Agnihotry, S. Chandra, and V. G. Bhode, *Mol. Cryst. Liq. Cryst.*, **104**, 161 (1984).
19) J. Tanno, K. Itoh, A. Tsuji, and K. Hori, *J. Mol. Struct.*, in press.
20) H. Wu and K. Hori, unpublished data.
21) C. Johnson, "ORTEP, Report ORNL-3794," Oak Ridge National Laboratory, Tennessee (1965).
22) P. Zugenmaier and A. Heiske, *Liq. Cryst.*, **15**, 835 (1993).
23) E. von Sydow, *Ark. Kemi*, **9**, 231 (1955).
24) H. M. M. Shearer and V. Vand, *Acta Crystallogr.*, **9**, 379 (1956).